Nickel(II)-Imprinted Monolithic Columns for Selective Nickel Recognition

Ebru Çubuk Demiralay,[1] Muge Andac,[2] Rıdvan Say,[3] Guleren Alsancak,[1] Adil Denizli[2]

[1]*Department of Chemistry, Suleyman Demirel University, Isparta, Turkey*
[2]*Department of Chemistry, Hacettepe University, Ankara, Turkey*
[3]*Department of Chemistry, Anadolu University, Eskişehir, Turkey*

Received 23 November 2009; accepted 16 February 2010
DOI 10.1002/app.32269
Published online 12 May 2010 in Wiley InterScience (www.interscience.wiley.com).

ABSTRACT: Ni^{2+}-imprinted monolithic column was prepared for the removal of nickel ions from aqueous solutions. *N*-Methacryloyl-L-histidine was used as a complexing monomer for Ni^{2+} ions in the preparation of the Ni^{2+}-imprinted monolithic column. The Ni^{2+}-imprinted poly(hydroxyethyl methacrylate-*N*-methacryloyl-L-histidine) (PHEMAH) monolithic column was synthesized by bulk polymerization. The template ion (Ni^{2+}) was removed with a 4-(2-pyridylazo) resorcinol (PAR):NH_3— NH_4Cl solution. The water-uptake ratio of the PHEMAH–Ni^{2+} monolith increased compared with PHEMAH because of the formation of nickel-ion cavities in the polymer structure. The adsorption of Ni^{2+} ions on both the PHEMAH–Ni^{2+} and PHEMAH monoliths were studied. The maximum adsorption capacity was 0.211 mg/g for the PHEMAH–Ni^{2+} monolith. Fe^{3+}, Cu^{2+}, and Zn^{2+} ions were used as competitive species in the selectivity experiments. The PHEMAH–Ni^{2+} monolithic column was 268.8, 25.5, and 10.4 times more selective than the PHEMAH monolithic column for the Zn^{2+}, Cu^{2+}, and Fe^{3+} ions, respectively. The PHEMAH–Ni^{2+} monolithic column could be used repeatedly without a decrease in the Ni^{2+} adsorption capacity. © 2010 Wiley Periodicals, Inc. J Appl Polym Sci 117: 3704–3714, 2010

Key words: adsorption; molecular imprinting; molecular recognition

INTRODUCTION

Nickel is a metallic element that is naturally present in the earth's crust. Nickel compounds are also found in soils and are present in both insoluble forms, such as sulfides and silicates, and in a number of soluble forms.[1] Natural sources of atmospheric nickel include dusts from volcanic emissions and the weathering of rocks and soils. Natural sources of aqueous nickel derive from biological cycles and soluble nickel compounds from soils. Because of their unique physical and chemical properties, metallic nickel and its compounds are widely used in modern industry. Nickel compounds are used in electroplating and electroforming and for the production of nickel–cadmium batteries and electronic equipment. Nickel alloys, such as stainless steel, are used in the production of tools, machinery, armaments, and appliances. The high consumption of nickel-containing products inevitably leads to environmental pollution by nickel and its byproducts at all stages of production, recycling, and disposal. The global input of nickel into the human environment is approximately 150,000 metric tons per year from natural sources and 180,000 metric tons per year from anthropogenic sources, including emissions from fossil fuel consumption and the industrial production, use, and disposal of nickel compounds and alloys.[2,3]

Human exposure to nickel occurs primarily via inhalation and ingestion. Significant amounts of nickel in different forms may be deposited in the human body through occupational exposure and diet over a lifetime.[4–7] It is known; however, that exposure to nickel compounds can have adverse effects on human health. A nickel allergy in the form of contact dermatitis is the most common and well-known reaction. Although the accumulation of nickel in the body through chronic exposure can lead to lung fibrosis and cardiovascular and kidney diseases, the most serious concerns relate to nickel's carcinogenic activity. Epidemiological studies have clearly implicated nickel compounds as human carcinogens on the basis of a higher incidence of lung and nasal cancer among nickel mining, smelting, and refinery workers.[8] In various animal models, nickel compounds induce tumors at virtually any site of administration. Additionally, insoluble nickel compounds such as nickel subsulfide efficiently transform rodent and human cells *in vitro*. On the basis of these observations, the International Agency

Correspondence to: A. Denizli (denizli@hacettepe.edu.tr).
Contract grant sponsor: Research Fund of Süleyman Demirel University (1203-D-05; Isparta-Turkey).

for Research on Cancer (IARC) evaluated the carcinogenicity of nickel in 1990.[9] All nickel compounds except for metallic nickel were classified as carcinogenic to humans.[1]

In recent years, molecular imprinting has attracted considerable interest in many areas of chemistry, biochemistry and biotechnology. In the field of chemistry, especially in analysis and separation science, molecularly imprinted materials have received increasing attention because of their high selectivity and affinity for the target molecules.[10,11] Molecular imprinting is a rapidly developing technique for the preparation of polymers having specific recognition properties that can selectively recognize the template molecules in the presence of compounds with structures and functionalities similar to that of the template.[12] *Molecularly imprinted polymers* (MIPs) are artificially synthesized macromolecular materials with a prearrangement of structure and specific recognition ability.[13] MIPs have been used as chromatographic media, sensors, artificial antibodies and catalysts.[14–16] Different approaches have been reported so far for metal-ion-imprinted materials.[17–22] These imprinted materials have been prepared in the form of particles or beads, which were then packed into columns.[23,24] However, MIPs can be prepared by bulk polymerization, where the resultant monolithic columns consist of a single piece of highly porous material. The pores inside the monolith are open and form a highly interconnected network of channels; this leads to a reduced diffusional mass-transfer resistance and facilitates convective transport.[25]

This article deals with the preparation of nickel-ion-imprinted monolithic columns, which can be used for the removal of nickel ions from aqueous solutions. *N*-Methacryloyl-L-histidine (MAH) was used as a complexing monomer for the preparation of Ni^{2+}-imprinted monolithic column. Ionic interactions between Ni^{2+} and the imidazole nitrogen atom, oxygen and peptide nitrogen atom in the MAH structure were the goal. PHEMAH was selected as the basic matrix, which had hydrophilic characteristics and high chemical and mechanical stabilities for column applications.[26,27] In this study, the Ni^{2+}-imprinted poly(hydroxyethyl methacrylate-*N*-methacryloyl-L-histidine) (PHEMAH) monolithic column was prepared by *in situ* polymerization, where there was no need to grind and sieve to form particles for column packing. The Ni^{2+}-imprinted PHEMAH monolithic column was characterized and used for the selective adsorption of Ni^{2+} ions from an aqueous solution. Ni^{2+} adsorption on the MIPs and selectivity studies of Ni^{2+} ions versus other interfering metal ions (Zn^{2+}, Cu^{2+}, and Fe^{3+}) were examined.

EXPERIMENTAL

Materials

L-Histidine and methacryloyl chloride were supplied from Sigma (St Louis, MO). Hydroxyethyl methacrylate (HEMA) and ethylene glycol dimethacrylate were obtained from Fluka A. G. (Buchs, Switzerland), distilled under reduced pressure in the presence of a hydroquinone inhibitor, and stored at 4°C until use. 4-(2-Pyridylazo) resorcinol (PAR) was supplied by Dionex Corp. (Munich, Germany) 4-(2-Hydroxyethyl)-1-piperazine ethanesulfonic acid was supplied from Sigma (St. Louis, MO). Nickel, iron, copper, and zinc stock solutions (1000 mg/L) were obtained from SCP Science. All other chemicals were reagent grade and were purchased from Merck AG (Darmstadt, Germany). All water used in the adsorption experiments was purified with a Barnstead ROpure LP reverse-osmosis unit (Dubuque, IA) with a high-flow cellulose acetate membrane (Barnstead D2731) followed by a Barnstead D3804 NANOpure organic/colloid-removal and ion-exchange, packed-bed system.

Preparation of the complex monomer (MAH–Ni^{2+})

The synthesis of MAH was adapted from a procedure reported by elsewhere.[28] The MAH–Ni^{2+} monomer–template complex was formed by the slow addition of MAH monomer (0.09 mmol) into a Ni^{2+} solution [0.045 mmol; Ni^{2+} source: $Ni(NO_3)_2{\cdot}5H_2O$] at room temperature by constant stirring (250 rpm) for 3 h. The newly prepared monomer–metal complex (MAH–Ni^{2+}) was filtered off, washed with 250 mL of water, and dried in a vacuum oven at 50°C for 24 h.

Preparation of the PHEMAH–Ni^{2+} monolithic column

The Ni^{2+}-imprinted PHEMAH (PHEMAH–Ni^{2+}) monolith was prepared by *in situ* polymerization in a closed-bottom syringe in the presence of potassium persulfate as the initiator. Briefly, 15 mg of potassium persulfate and 45 mg of 4-(2-hydroxyethyl)-1-piperazine ethanesulfonic acid were dissolved in a mixture of HEMA (1.0 mL) and MAH–Ni^{2+} complex (0.1 mmol). Toluene (0.750 mL) and ethylene glycol dimethacrylate (0.250 mL) were included as the diluent (as a pore former) and crosslinker, respectively. A monomer mixture (4 mL), including the initiator and the porogenic diluent, was transferred into a closed-bottom syringe (4 mL, inside diameter = 1.0 cm); this was followed by a sonication step to obtain a clear solution, which was then purged with nitrogen gas for 15 min. The polymerization was allowed to proceed at 75°C in a water bath for 1 h. As a control, the nonimprinted (PHEMAH) monolithic column was synthesized in the absence of Ni^{2+} ions

by the same polymerization procedure. After the polymerization was completed, water was pumped through the column at a flow rate of 0.5 mL/min to remove the unreacted monomers and porogenic diluents present in the monolith. The template (Ni^{2+} ions) was removed by a PAR:NH_3–NH_4Cl (pH 10) buffer system for 2 h at room temperature. This procedure was repeated several times until the Ni^{2+} ions could not be detected in washing solution. The template-free monolith was cleaned with 0.1*M* HNO_3 and deionized water. When not in use, the resulting monolithic column was kept under refrigeration in a 0.02% sodium azide (NaN_3) solution to prevent microbial contamination.

Characterization studies

The surface structure of the monolith sample was visualized and examined by scanning electron microscopy (SEM). After the monolith sample was dried at 25°C for 7 days, tiny fragments of the monoliths were mounted on SEM sample holders, on which they were sputter-coated for 2 min. The sample was then consecutively mounted in a scanning electron microscope (Jeol JSM-5600; Tokyo, Japan) to visualize the surface structures of each monolith at desired magnification levels.

The surface area of the monolith sample was determined by a multipoint Brunauer–Emmett–Teller (BET) apparatus (Quantachrome, Nova 2200E; Florida). The monolith (0.5 g) was placed in a sample holder of BET and degassed by passage through N_2 gas at 150°C for 1 h. The adsorption of the N_2 gas was performed at −210°C, whereas its desorption was performed at room temperature. Experimental values obtained from the desorption step were used to calculate the specific surface area of the monolith.

The water-uptake ratio was determined in deionized water. The water-uptake experiment was conducted as follows: the dry monolith was carefully weighed before it was soaked in a 50-mL vial containing distilled water. The vial was then placed into an isothermal water bath at 25°C for 2 h, after which the wet-monolith sample was taken out of the vial, wiped with filter paper, and weighed. The water content of the monolith was calculated with the weight of the monolith before and after the uptake of water.

The elemental analysis of monolith was implemented on a Leco elemental analyzer (model CHNS-932; St. Joseph, MI) to evaluate the MAH incorporation amount in the monoliths.

Fourier transform infrared (FTIR) spectroscopy was studied on an FTIR instrument (Shimadzu IR Prestige-21, Japan) to determine the functional groups detected in the range 4000–400 cm^{-1} for the MAH monomer, the MAH–Ni^{2+} complex, and the PHEMAH–Ni^{2+} sample in the solid state.

Assay of nickel in aqueous solutions

PAR is commonly used as a chromogenic reagent. It reacts with many metal ions, particularly with nickel, forming intense red-colored complexes in alkaline media. All complexation reactions of PAR with metal ions are strongly dependent on the pH of the solution because PAR is an organic ampholyte, which, in acidic media, can easily attract a proton to its pyridine nitrogen atom; in basic media, its *o*-hydroxyl group can easily dissociate.[29] Our method was based on the reaction between the analyte and PAR at pH 10.0. In all mixtures, the PAR concentration (mol/L) was kept equal to six-fold the sum of metal concentrations (moles per liter) in the most concentrated calibration mixture, that is, [PAR]/[Metals] $\geq$ 6. Briefly, the solution for analysis was prepared by the successive addition of aliquots of Ni^{2+}-ion solution, 4.75 mL of NH_3—NH_4Cl buffer solution (pH 10), and 2.65 mL of 2.5×10^{-4} *M* PAR solution in ethanol to a 10 mL volumetric flask. Then, water was added, and the solution was sonicated for 2 min. The absorbance was measured against a corresponding reagent blank. The concentration of the complex was determined by an ultraviolet–visible spectrophotometer (Shimadzu UV-1601; Tokyo, Japan) at a wavelength of 494 nm.

The limit of detection (LOD) and limit of quantification (LOQ) were calculated from the following equations:

$$\mathrm{LOD} = 3.3\frac{s}{m} \quad (1)$$

$$\mathrm{LOQ} = 10\frac{s}{m} \quad (2)$$

where s is the standard deviation of response and m is the slope of the corresponding calibration curve.

Adsorption of Ni^{2+} ions from aqueous solutions

The adsorption of Ni^{2+} ions on both the PHEMAH–Ni^{2+} and PHEMAH monoliths from aqueous solutions were studied in a continuous system. The effect of the flow rate on Ni^{2+} adsorption was implemented in the range 0.5–3.5 mL/min. The pH of the solution was changed between 4.0 and 8.0 to determine the effect of pH. The effect of the equilibrium concentration on Ni^{2+}-ion adsorption was studied in the range 5–100 mg/L. After the desired treatment period, the concentration of the Ni^{2+} ions in the aqueous phase was determined by the PAR method, as described earlier. The experiments were performed in replicates of three, and the samples were also analyzed in replicates of three. For each set of data present, standard statistical methods were used to determine the mean values and standard

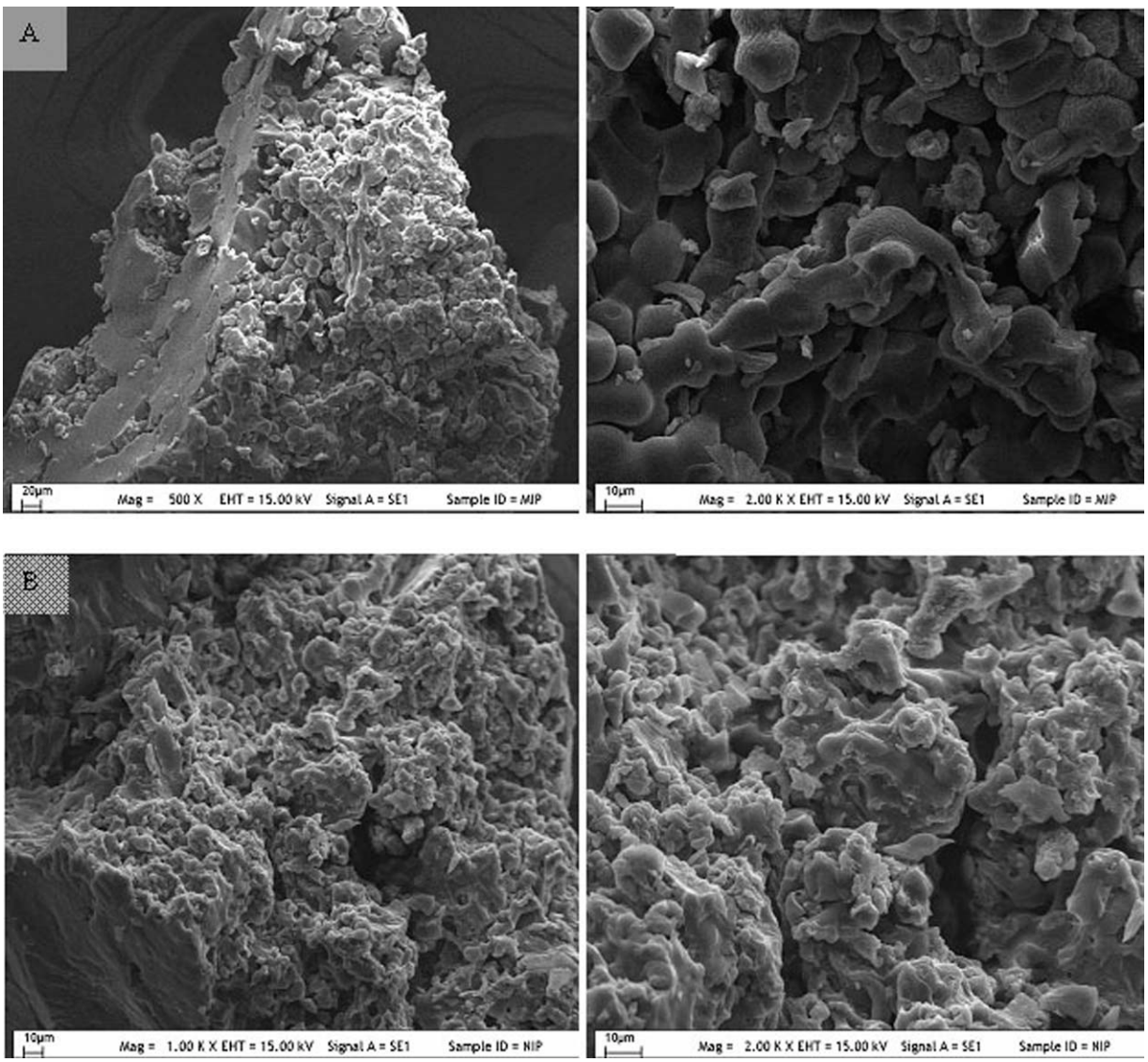

Figure 1 SEM micrographs of the (A) PHEMAH–Ni^{2+} and (B) PHEMAH monoliths.

deviations. Confidence intervals of 95% were calculated for each set of samples to determine the margin of error. The amount of Ni^{2+} adsorbed on unit mass of each monolith was evaluated with a mass balance approach.

Selectivity experiments

The nickel (Ni^{2+}; Atomic weight (A_w) = 58.69 g/mol, ionic radius = 69 pm) specificity of the PHEMAH–Ni^{2+} monolith was compared with the competitive adsorption of zinc (Zn^{2+}; A_w = 65.39 g/mol, ionic radius = 74 pm), iron (Fe^{3+}; A_w = 55.85 g/mol, ionic radius = 64 pm), and copper (Cu^{2+}; A_w = 63.55 g/mol, ionic radius = 72 pm). The equilibrium concentration of the competitive ions (i.e., Zn^{2+}, Fe^{3+}, and Cu^{2+}) was 30 mg/L in 0.1% $HClO_4$, (v/v; pH 6.0). The PHEMAH–Ni^{2+} and PHEMAH monoliths were treated with these competitive ions. After adsorption equilibrium, the concentration of Zn^{2+}, Fe^{3+}, and Cu^{2+} ions in the remaining solution was measured with a Dionex BIO-LC and postcolumn reactor. The column was an ion pack CG5A Guard (P/N 046104) and IonPac CS5A analytical column (P/N 046100) (Dionex Corp., Munich, Germany). The eluent was MetPac PDCA eluent concentrate (P/N 046088) (Dionex Corp., Munich, Germany). The flow rate was 1.2 mL/min, and the expected backpressure was 1700–1900 psi. The postcolumn reagent was 0.5 m*M* PAR (P/N 39672) in MetPac PAR postcolumn reagent diluent (P/N 046094) (Dionex Corp., Munich, Germany) with a postcolumn reagent flow rate of 0.6 mL/min.

The distribution of Cu^{2+}, Fe^{3+}, and Zn^{2+} with respect to Ni^{2+} was obtained from the equilibrium binding data according to eq. (3):

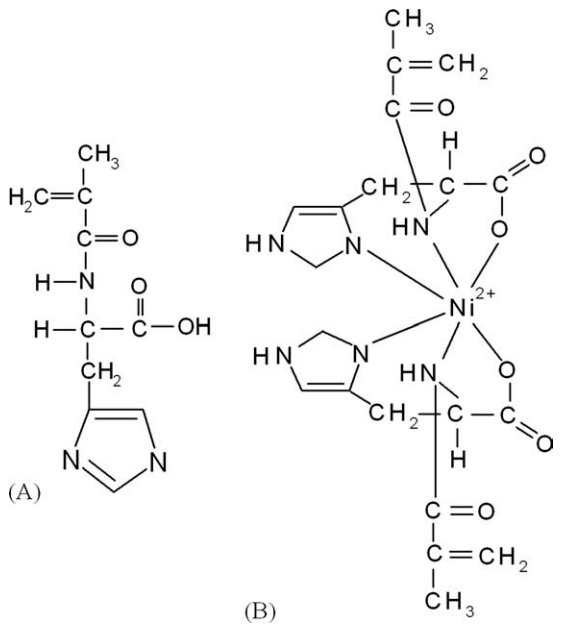

Figure 2 (A) Molecular formula of the MAH monomer. (B) Possible structure of the MAH–Ni^{2+} complex monomer.

$$K_d = \left[\frac{(C_i - C_f)}{C_f}\right] \times \frac{V}{m} \quad (3)$$

where K_d is the distribution coefficient (mL/g); C_i and C_f are the initial and final concentrations of the metal ions (μmol/mL), respectively; V is the volume of the solution (mL); and m is the mass of monolith used (g). The selectivity coefficient (k) was calculated according to eq. (4):

$$k = \frac{K_{d(\text{template ion})}}{K_{d(\text{interferent ion})}} \quad (4)$$

where $K_{d(\text{template ion})}$ and $K_{d(\text{interferent ion})}$ are the distribution coefficients. A comparison of the k values of the PHEMAH–Ni^{2+} monoliths with the metal ions allowed us to estimate the effect of imprinting on selectivity. The relative selectivity coefficients (k') for the PHEMAH–Ni^{2+} and PHEMAH monoliths were also calculated by eq. (5):

$$k = \frac{k_{\text{imprinted}}}{k_{\text{control}}} \quad (5)$$

where $k_{\text{imprinted}}$ and k_{control} are the selectivity coefficients.

Desorption and repeated use

The desorption of Ni^{2+} ions was studied with PAR:NH_3—NH_4Cl (pH 10) and water (27 : 48 : 25 v/v %) mixture. The monolithic column (4 mL, inside diameter = 1.0 cm) was stable at pH 10.0. In a continuous desorption experiment, 20 mL of the desorption agent was pumped through the monolithic column at a flow rate of 0.5 mL/min for 2 h. The desorption ratio was calculated from the amount of Ni^{2+} ions adsorbed on the monolith and the final Ni^{2+}-ion concentration in the desorption medium. The concentration of Ni^{2+} ions in desorption medium was determined by the PAR method. To test the reusability of the PHEMAH–Ni^{2+} monolith, the Ni^{2+}-ion adsorption–desorption procedure

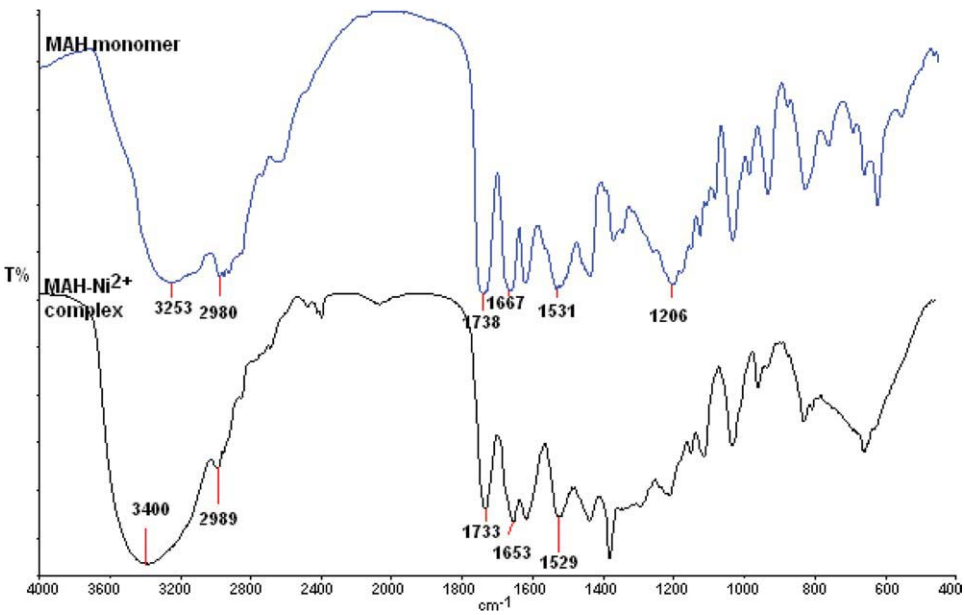

Figure 3 FTIR spectra of MAH and the MAH–Ni^{2+} complex monomer. [Color figure can be viewed in the online issue, which is available at www.interscience.wiley.com.]

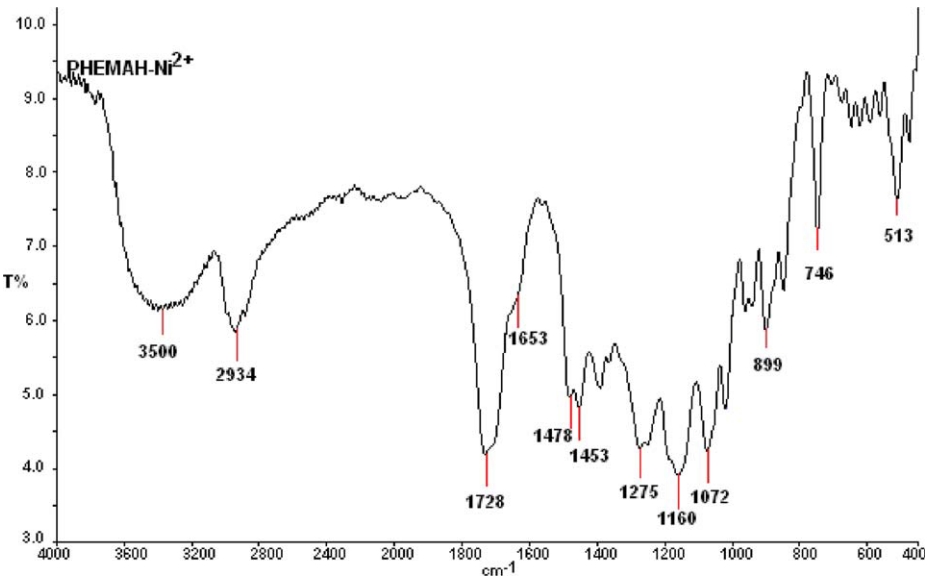

Figure 4 FTIR spectra of the PHEMAH–Ni^{2+} monolith. [Color figure can be viewed in the online issue, which is available at www.interscience.wiley.com.]

was repeated five times with the same monolith. To regenerate it after desorption, the monolith was washed with 0.1*M* HNO_3 and deionized water.

RESULTS AND DISCUSSION

Characterization of the PHEMAH–Ni^{2+} monolithic columns

The specific surface area was found to be 45.8 m^2/g for PHEMAH–Ni^{2+} and 32.3 m^2/g for PHEMAH, respectively, by the BET method. The equilibrium swelling ratio was measured as 72.8% for PHEMAH–Ni^{2+} and 64.9% for PHEMAH. Compared with that of the PHEMAH monolith, the water-uptake ratio of the PHEMAH–Ni^{2+} monolith increased because of the formation of imprinted nickel-ion cavities in the polymer structure.

The porous character of the PHEMAH–Ni^{2+} and PHEMAH monoliths were exemplified by SEM photographs (Fig. 1). Both the PHEMAH–Ni^{2+} and PHEMAH monoliths had porous, rough surfaces and good flow properties for column applications.

The incorporations of MAH with nitrogen stoichiometry were determined to be 33.4 and 28.5 μmol/g of polymer for the PHEMAH–Ni^{2+} and PHEMAH monoliths, respectively. HEMA and other chemicals used in the polymerization process did not contain nitrogen. The amount of nitrogen determined by elemental analysis originated only from the MAH groups incorporated into the polymeric structure.

Characterization of the Ni^{2+}–MAH complex formation

The molecular formulas of the MAH monomer and MAH–Ni^{2+} complex are shown in Figure 2. A metal coordination complex was formed between the Ni^{2+} ions and the imidazole nitrogen atom, oxygen, and peptide nitrogen atom in the MAH structure. The Ni^{2+}–MAH coordination complex was an octahedral structure.

To confirm complex formation between Ni^{2+} and the MAH monomer, FTIR measurements were performed. The FTIR spectrum of MAH with the characteristic amide I and amide II stretching vibration bands at 1667 and 1531 cm^{-1}, carbonyl band at 1739 cm^{-1}, and C—O bending absorption band at 1206 cm^{-1} is shown in Figure 3. In the analyzed IR spectra of the complex, the characteristic amide I and amide II stretching vibration bands at 1667 and 1531 cm^{-1} shifted to down 1653 and 1529 cm^{-1} (Fig. 3). The appearance of a significant broad peak at 661 cm^{-1} in the FTIR spectrum of the MAH–Ni^{2+}

TABLE I
Calibration Data for Ni^{2+}–PAR Complex

Sample	Linearity range (μg/mL)	Slope	Intercept	SD of the slope	SD of the intercept	R^2	LOD (μg/mL)	LOQ (μg/mL)
Ni^{2+}	0.255–0.638	1.34	0.162	0.031	0.014	0.999	0.024	0.072

SD = standard deviation.

complex also indicated the presence of Ni^{2+} ions in the complex.

The MAH–Ni^{2+} complex was incorporated into the polymer structure by bulk polymerization. The FTIR spectrum of the PHEMAH–Ni^{2+} monolith had the characteristic stretching vibration band of hydrogen-bonded alcohol, O—H, around 3500 cm^{-1}, carbonyl at 1728 cm^{-1}, C—O bending absorption band at 1275 cm^{-1}, and amide I and amide II absorption bands at 1635 and 1478 cm^{-1}, respectively (Fig. 4).

Assay of nickel in aqueous solution

The nickel-ion concentration in aqueous solution was detected by a method that was based on the reaction between the analyte and PAR at pH 10.0, as described earlier. The absorbance was measured against a corresponding reagent blank at 494 nm. The calibration data was constructed by the plotting of absorbance versus standard concentration (Table I). The LOD for nickel ions was determined as 0.024 μg/mL.

Adsorption of Ni^{2+} from aqueous solutions

Effect of the flow rate

The adsorbed amounts of Ni^{2+} ions at different flow rates are given in Figure 5. The adsorbed amount of Ni^{2+} ions decreased significantly from 0.21 to 0.08 mg/g as the flow rate increased from 0.5 to 3.5 mL/min. This could be explained by ligand–template (i.e., MAH–Ni^{2+}) interaction, which would have a faster dissociation rate compared to the association rate, because the template ions (i.e., Ni^{2+}) would have passed through the monolithic column without binding at a high flow rate. The contact time in the column was longer as the flow rate decreased; the diffusion then became more effective.

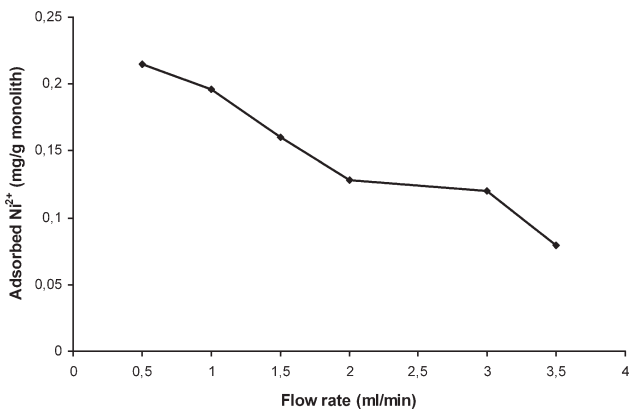

Figure 5 Effect of the flow rate on the adsorption of Ni^{2+} ions of the PHEMAH–Ni^{2+} monolith (Ni^{2+}-ion concentration = 30 mg/L, total volume = 20 mL, polymer amount = 800 mg, temperature = 20°C).

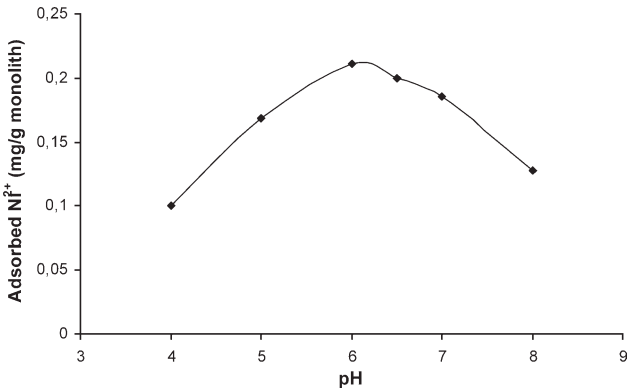

Figure 6 Effect of pH on the adsorption of Ni^{2+} ions of the PHEMAH–Ni^{2+} monolith (Ni^{2+}-ion concentration = 30 mg/L, flow rate = 0.5 mL/min, total volume = 20 mL, polymer amount = 800 mg, temperature = 20°C).

Thus, the Ni^{2+} ions had more time to diffuse and bind the nickel-ion cavities in the monolithic column, and a better adsorption capacity was obtained.

Effect of pH

The adsorption effectivity of Ni^{2+} ions was extremely dependent on pH. Ni^{2+} adsorption onto the PHEMAH–Ni^{2+} monolith was measured at different pH values of buffer solutions (pH 4.0–8.0). The effect of pH on Ni^{2+} adsorption is shown in Figure 6. As shown, the maximum Ni^{2+} adsorption amount was obtained in pH 6.0 phosphate buffer; this was the isoelectric point of the imidazole side chain (imidazole group pK_a = 5.97) of the MAH monomer. This suggested that the Ni^{2+} ions electrostatically interacted with the imidazole side chain of MAH. This way, the binding should not have decreased with increasing pH above 6.0, where both the imidazole ring and carboxy group were depronated; this, hence, promoted binding. The decrease in the binding affinity could be explained by hydroxide ions, which started competing for Ni^{2+} ions at high pH values and prevented their binding to the adsorbent.

Effect of the equilibrium concentration of Ni^{2+} ions

The adsorbed amount of Ni^{2+} ions on the PHEMAH–Ni^{2+} monolithic column was dependent on the equilibrium concentration of Ni^{2+} ions. The adsorption amount increased with increasing concentration of Ni^{2+} ions, and a saturation value was achieved at a concentration of 30 mg/L, which represented the saturation of the active binding nickel-ion cavities of the PHEMAH–Ni^{2+} monolith (solid line in Fig. 7). Mass transfer limitations were also overcome by a high driving force, which was the concentration difference of Ni^{2+} between the liquid

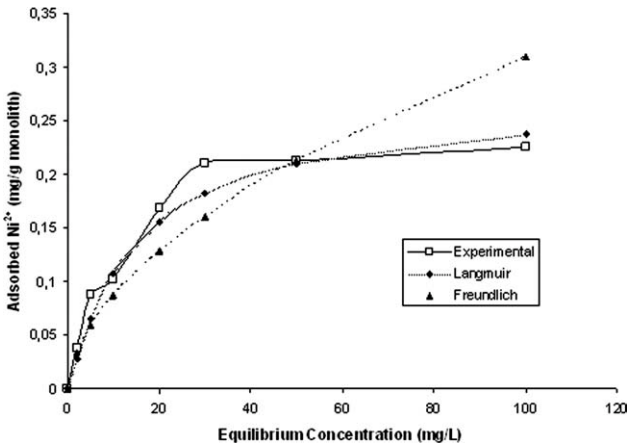

Figure 7 Experimental data of the absorbed Ni^{2+} ions onto the PHEMAH–Ni^{2+} monolith compared to the Langmuir and Freundlich isotherms (pH 6.0, flow rate = 0.5 mL/min, total volume = 20 mL, polymer amount = 800 mg, temperature = 20°C).

and the solid phases in the case of high Ni^{2+}-ion concentration. The maximum adsorbed amount of Ni^{2+} ions was 0.21 mg/g monolith.

Two important physicochemical aspects for the evaluation of the adsorption process as a unit operation are the kinetics and the equilibria of adsorption. The modeling of the equilibrium data was done with the Langmuir and Freundlich isotherms.[30] The Langmuir and Freundlich isotherms are represented in eqs. (6) and (7), respectively:

$$q = q_{\max} b \frac{C_e}{(1 + bC_e)} \tag{6}$$

$$q = K_F C_e^{1/n} \tag{7}$$

where q is the Langmuir adsorption capacity (mg/g), C_e is the equilibrium Ni^{2+} concentration (mg/mL), b is the constant related to the affinity binding sites, K_F is the Freundlich constant, and n is the Freundlich exponent.

In Figure 7, the experimental adsorption behavior is compared with Langmuir and Freundlich adsorption isotherms. The experimental data tended to agree more with a Langmuir adsorption fit rather than the Freundlich isotherm because the correlation coefficient (R^2) was high (0.99). The maximum amount of adsorption (0.21 mg/g) obtained from experimental results was also very close to the calculated q (0.27 mg/g). Table II shows the experimental and calculated results. We concluded that the adsorbed Ni^{2+} ions onto the PHEMAH–Ni^{2+} monolith showed a monolayer adsorption behavior.

The factors affecting adsorption mechanism, such as mass transfer and the chemical reaction, were investigated on the basis of two different kinetic models. The kinetic models (pseudo-first-order and pseudo-second-order equations) could be used in this case with the assumption that the measured concentrations were equal to the adsorbent surface concentrations. The first-order rate expression of Lagergren is one of the most widely used for the adsorption of a solute from a liquid solution.[31]

The pseudo-first-order kinetic model is expressed by eq. (8):

$$\log(q_e - q_t) = \log q_e - \frac{(k_1 t)}{2.303} \tag{8}$$

where q_e is the experimental amount of Ni^{2+} adsorbed at equilibrium (mg/g), q_t is the amount of Ni^{2+} adsorbed at time t (mg/g), and k_1 is the rate constant of the pseudo-first-order adsorption (min^{-1}). A straight line of $\log(q_e - q_t)$ versus t suggested the applicability of this kinetic model. Also, in many cases, the pseudo-first-order equation of Lagergren did not fit well to the whole range of contact times and was generally applicable over the initial stage of the adsorption processes.

The pseudo-second-order kinetic model is expressed by eq. (9):

$$\left(\frac{t}{q_t}\right) = \left(\frac{1}{k_2 q_e^2}\right) + \left(\frac{1}{q_e}\right) t \tag{9}$$

where k_2 is the rate constant of the pseudo-second-order adsorption [g (mg min)$^{-1}$]. If the pseudo-second-order kinetics were applicable, the plot of t/q versus t would show a linear relationship. The pseudo-second-order kinetic model is favorable when the adsorption behavior over the whole range of adsorption is in agreement with the chemical sorption being the rate-controlling step.[32] The time interval was changed in the range 0–60 min for the both pseudo-first-order and pseudo-second-order adsorption mechanisms.

TABLE II
Langmuir and Freundlich Adsorption Isotherm Constants

	Experimental	Langmuir constants			Freundlich constants		
	q_{ex} (mg/g)	q_{max} (mg/g)	b (g/mg)	R^2	K_F	n	R^2
PHEMAH–Ni^{2+} monolith	0.21	0.27	67.83	0.997	1.0812	0.54	0.944

q_{ex} = experimental adsorption capacity; q_{max} = Langmuir maximum adsorption capacity.

TABLE III
k_1 and k_2 Values for the PHEMAH–Ni^{2+} Monolith

Equilibrium concentration (mg/L)	Experimental	Pseudo-first-order kinetics			Pseudo-second-order kinetics		
	q_{ex} (mg/g)	k_1 (min^{-1})	q_e (mg/g)	R^2	k_2 [g (mg min)$^{-1}$]	q_e (mg/g)	R^2
30	0.211	0.007	0.739	0.988	0.091	0.312	0.998

q_{ex} = experimental adsorption capacity.

As shown in Table III, R^2 in the linear plot of $-\log(q_e - q_t)$ versus t for the pseudo-first-order equation was lower than R^2 in the linear plot of t/q_t versus t for the pseudo-second-order equation. The theoretical q_e value was slightly more different from the experimental value (0.312 mg/g). These results show that this adsorbent system was not so well described by pseudo-first-order kinetic model. However, the theoretical q_e value calculated from the pseudo-second-order kinetic model was very close to the experimental value, and R^2 was much higher than that in the pseudo-first-order kinetic model. By these results, the pseudo-second-order adsorption mechanism was predominant for the PHEMAH–Ni^{2+} monolith, and the overall rate of the Ni^{2+} adsorption process appeared to be controlled by a chemical process.

Selectivity experiments

The competitive adsorption of Cu^{2+}/Ni^{2+}, Fe^{3+}/Ni^{2+} and Zn^{2+}/Ni^{2+} from their mixtures were also studied in a continuous system. Cu^{2+}, Fe^{3+} and Zn^{2+} were chosen as competitive metal ions. After adsorption equilibrium was achieved, the concentrations of Cu^{2+}, Fe^{3+} and Zn^{2+} ions in the remaining solution were measured by BIO-LC (Dionex BIO-LC and postcolumn reactor). The target ion (Ni^{2+}) and competitive ions (Cu^{2+}, Fe^{3+} and Zn^{2+}) were separated by an IonPac analytical column, as described earlier.

Table IV summarizes the K_d, k, and k', values of Cu^{2+}, Fe^{3+} and Zn^{2+} with respect to Ni^{2+}. A comparison of the K_d values for the PHEMAH–Ni^{2+} samples with the control samples showed an increase in K_d for Ni^{2+}, whereas K_d decreased for Fe^{3+}, Cu^{2+}, and Zn^{2+}. k' is an indicator for the expression of the metal-binding affinity of recognition sites to imprinted Ni^{2+} ions. These results show that the k' values of PHEMAH–Ni^{2+} for Ni^{2+}/Zn^{2+}, Ni^{2+}/Cu^{2+}, and Ni^{2+}/Fe^{3+} in single-ion media were 1.6, 2.4 and 2.1 times greater than the PHEMAH monolith, respectively (Table IV). In addition to these results, the k' values of the PHEMAH–Ni^{2+} monolith for Ni^{2+}/Zn^{2+}, Ni^{2+}/Cu^{2+} and Ni^{2+}/Fe^{3+} in template/competitive ion pairs media were 268.8, 25.5, and 10.4 times greater than the PHEMAH monolith, respectively (Table IV).

Figure 8 illustrates the adsorbed template and competitive ions in both the PHEMAH–Ni^{2+} and PHEMAH monoliths. As shown in Figure 8(A), the Ni^{2+} ions had good selectivity toward the competitive ions (i.e., Cu^{2+}, Fe^{3+} and Zn^{2+}). The results show that the competitive adsorption of Ni^{2+} ions increased in the multiple-ion media [Fig. 8(B)]. The adsorption capacity of the PHEMAH monolith was considerably higher than the PHEMAH–Ni^{2+} ones. This could have been due to the nonspecific interactions between the Ni^{2+} ions and MAH molecules incorporated into the PHEMAH monolith. However, the relative selectivity of the PHEMAH–Ni^{2+} monolith was not affected by this phenomenon (Table IV).

Desorption and repeated use

The desorption of the Ni^{2+} ions from the PHEMAH–Ni^{2+} monolith was performed in a continuous system. Different factors were probably involved in determining the rates of Ni^{2+} desorption, such as

TABLE IV
K_d, k, and k' Values of Cu^{2+}, Fe^{3+}, and Zn^{2+} with Respect to Ni^{2+}

Metal ion	PHEMAH		PHEMAH–Ni^{2+}		
	K_d (mL/g)	k	K_d (mL/g)	k	k'
Ni^{2+}	5.43	—	13.58	—	—
Zn^{2+}	2.51	2.16	3.36	3.61	1.67
Cu^{2+}	0.77	7.02	0.81	16.79	2.39
Fe^{3+}	2.14	2.54	2.53	5.36	2.11
Ni^{2+}/Zn^{2+}	—	0.17	—	46.36	268.84
Ni^{2+}/Cu^{2+}	—	0.98	—	25.11	25.56
Ni^{2+}/Fe^{3+}	—	0.04	—	0.37	10.37

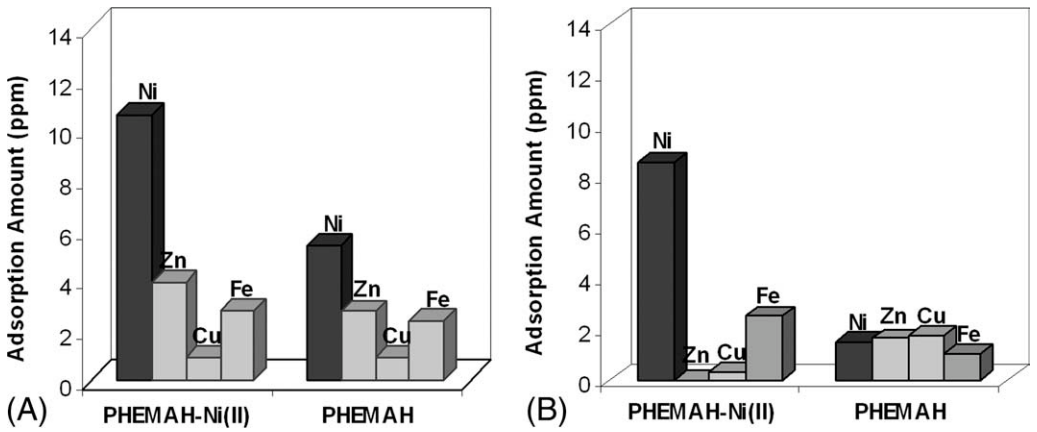

Figure 8 Adsorbed template and competitive ions both in the PHEMAH–Ni^{2+} and PHEMAH monoliths for the (A) single metal ions and (B) template/competitive ion pairs (i.e., Ni^{2+}/Zn^{2+}; flow rate = 0.5 mL/min; Ni^{2+}, Cu^{2+}, Fe^{3+} and Zn^{2+} concentrations = 30 mg/L; pH 6.0; total volume = 20 mL; polymer amount = 800 mg, temperature = 20°C).

the extent of the hydration of metal ions and the polymer microstructure. However, an important factor appeared to be binding strength. In this study, the desorption time was 45 min. The desorption ratio was high (up to 82%). To determine the reusability of the PHEMAH–Ni^{2+} and PHEMAH monoliths, adsorption–desorption cycles were repeated five times with the same PHEMAH–Ni^{2+} and PHEMAH monoliths. The adsorption capacity of the recycled PHEMAH–Ni^{2+} and PHEMAH monoliths could still be maintained at the fifth cycle (Fig. 9). We concluded that the PHEMAH–Ni^{2+} and PHEMAH monoliths could be used several times without decreases in their adsorption capacities.

CONCLUSIONS

MIPs are synthetic materials that mimic biological receptors in their specific recognition of analytes.[33] They possess several advantages over their biological counterparts, including low cost, simple and convenient preparation, storage stability, repeated operations without loss of activity, high mechanical strength, durability to heat and pressure and applicability in harsh chemical media.[34–36] In this study, MIPs were prepared by bulk polymerization. The specific surface area increased after template removal as a result of the formation of cavities. The adsorption of Ni^{2+} ions was established in 45 min. The adsorption difference between the PHEMAH–Ni^{2+} and PHEMAH monoliths was most probably due to the geometric shape affinity (or memory) of Ni^{2+} ions toward Ni^{2+} cavities in the PHEMAH–Ni^{2+} structure. The adsorption values increased with increasing concentration of Ni^{2+} ions, and a saturation value was achieved at an ion concentration of 30 mg/L, which represents the saturation of the active binding cavities on the PHEMAH–Ni^{2+} and PHEMAH monoliths. The Langmuir adsorption model could be applied in this affinity adsorbent system. k' was an indicator to express the adsorption affinity of recognition sites to the imprinted Ni^{2+} ions. A significant increase was observed in the selectivity of the PHEMAH–Ni^{2+} monolith when the adsorbent was prepared in the presence of the target ion. Finally, the PHEMAH–Ni^{2+} monolith could be used many times without a significant decrease in its adsorption capacity.

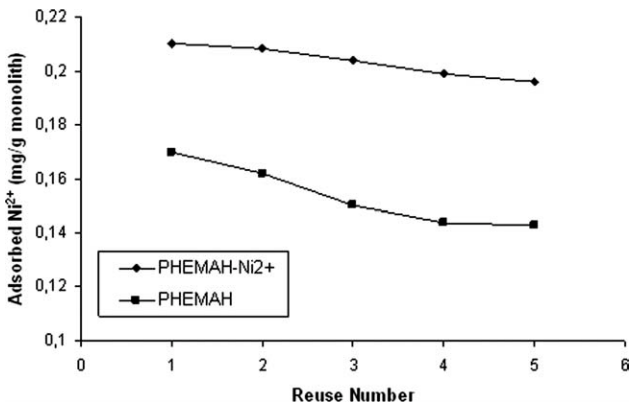

Figure 9 Adsorption–desorption cycle of the PHEMAH–Ni^{2+} and PHEMAH monoliths (flow rate = 0.5 mL/min, Ni^{2+}-ion concentration = 30 mg/L, pH 6.0, total volume = 20 mL, polymer amount = 800 mg, temperature = 20°C).

References

1. Garrett, R. G. In Natural Sources of Metals to the Environment; Centeno, J. A.; Collery, P.; Fernet, G.; Finkelman, R. B.; Gibb, H.; Etienne, J.-C., Eds.; John Libbey Eurotext: Paris, 2000.
2. Kasprzak, K. S.; Sunderman, F. W., Jr.; Salnikowa, K. Mutat Res 2003, 533, 67.
3. Sunderman, F. W., Jr. In Nickel, A. M.; Ihnat, M.; Stoeppler, M., Eds.; Wiley-VCH: Weinheim, 2004.
4. Denkhaus, E.; Salnikow, K. Crit Rev Oncol/Hematology 2002, 42, 35.

5. Dourson, M. Toxicology Excellence for Risk Assessment (TERA). Toxicological Review of Soluble Nickel Salts; prepared for the Metal Finishing Association of Southern California, Inc.; U. S. Environmental Protection Agency and Health Canada, Cincinnati, OH, 1999.
6. Cangul, H.; Broday, L.; Salnikow, K.; Sutherland, J.; Peng, W.; Zhang, Q.; Poltaratsky, V.; Yee, H.; Zoroddu, M.; Costa, M. Toxicol Lett 2002, 27, 69.
7. Costa, M.; Davidson, T. L.; Chen, H.; Ke, Q.; Zhang, P.; Yan, Y.; Huang, C.; Kluz, T. Mutat Res 2005, 592, 79.
8. Easton, D. F.; Peto J, Morgan, L. G.; Metcalfe, L. P.; Usher, V.; Doll, R. In Respiratory Cancer in Welsh Nickel Refiners: Which Nickel Compounds Are Responsible?; Nieboer, E.; Nriagu, J. O., Eds.; Wiley: New York, 1992.
9. International Agency for Research on Cancer. IARC Monographs on the Evaluation of Carcinogenic Risks to Humans; Chromium, Nickel and Welding 49, WHO Press, Lyon, France, 1990.
10. Andersson, L. I. J Chromatogr B 2000, 745, 3.
11. Jiang, X.; Jiang, N.; Zhang, H.; Liu, M. Anal Bioanal Chem 2007, 389, 355.
12. Yan, H.; Row, K. H. J Ind Eng Chem 2007, 13, 552.
13. Lin, L. Q.; Zhang, J.; Fu, Q.; He, L. C.; Li, Y. C. Anal Chim Acta 2006, 561, 178.
14. Sellergren, B. Molecularly Imprinted Polymers: Man-Made Mimics of Antibodies and Their Applications in Analytical Chemistry; Elsevier: Amsterdam, 2001.
15. Yan, M.; Ramström O. Molecularly Imprinted Materials; Marcel Dekker: New York, 2005.
16. Haginaka, J. J Chromatogr B 2008, 866, 3.
17. Andac, M.; Özyapı, E.; Şenel, S.; Say, R.; Denizli, A. Ind Eng Chem Res 2006, 45, 1780.
18. Andac, M.; Mirel, S.; Şenel, S.; Say, R.; Ersöz, A.; Denizli, A. Int J Biol Macromol 2007, 40, 159.
19. Yavuz, H.; Say, R.; Denizli, A. Mater Sci Eng C 2005, 25, 521.
20. Andac, M.; Say, R.; Denizli, A. J Chromatogr B 2004, 811, 119.
21. Say, R.; Birlik, E.; Ersöz, A.; Yılmaz, F.; Gedikbey, T.; Denizli, A. Anal Chim Acta 2003, 480, 251.
22. Araki, K.; Maruyama, T.; Kamiya, N.; Goto, M. J Chromatogr B 2005, 818, 141.
23. Ersöz, A.; Say, R.; Denizli, A. Anal Chim Acta 2004, 502, 91.
24. Romani, J. O.; Pineiro, A. M.; Barrera, P. B.; Esteban, A. M. Anal Chim Acta 2008, 630, 1.
25. Uzun, L.; Say, R.; Denizli, A. React Funct Polym 2005, 64, 93.
26. Denizli, A. J Appl Polym Sci 1999, 74, 655.
27. Denizli, A. J Chromatogr B 2002, 772, 357.
28. Bereli, N.; Uzun, L.; Yavuz, H.; Elkak, A.; Denizli, A. J Appl Polym Sci 2006, 101, 395.
29. Karipcin, F.; Kabalcilar, E. Acta Chim Slov 2007, 54, 242.
30. Finette, G. M. S.; Qui-Ming, M.; Hearn, M. T. W. J Chromatogr A 1997, 763, 71.
31. Cheung, C. W.; Porter, J. F.; Mckay, G. Water Res 2001, 35, 605.
32. Liang, Z. P.; Feng, Y. Q.; Liang, Z. Y.; Meng, S. X. Biochem Eng J 2005, 24, 65.
33. Karim, K.; Breton, F.; Rouillon, R.; Piletska, E. V.; Guerreiro, A.; Chianella, I.; Piletsky, S. A. Adv Drug Delivery Rev 2005, 57, 1795.
34. Lavignac, N.; Allender, C. J.; Brain, K. R. Anal Chim Acta 2004, 510, 139.
35. Vlatakis, G.; Andersson, L. I.; Müller, R.; Mosbach, K. Nature 1993, 361, 645.
36. Özcan, A. A.; Say, R.; Denizli, A.; Ersöz, A. Anal Chem 2006, 78, 7253.